STRUCTURAL INTEGRITY OF LARGE STEAM TURBINE ROTORS

by

Gary W. Rogers

Managing Engineer

and Director, Phoenix Office

Failure Analysis Associates

2234 South McClintock Drive

Tempe, Arizona

and

Clifford H. Wells

Vice President, Research and Development

and

Duane P. Johnson

Managing Engineer

Failure Analysis Associates

2225 East Bayshore Road

Palo Alto, California

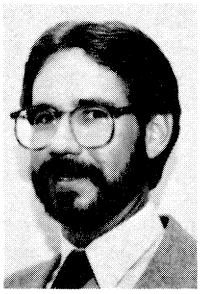

Gary W. Rogers is Director of the Phoenix office of Failure Analysis Associates and manages the analysis, laboratory and field testing of reciprocating and turbo machinery. His ten years' vibrations and dynamics experience has spanned oil, aerospace and utility industry applications.

As an exploration geophysicist for Shell Oil Company, Mr. Rogers developed random vibration analysis techniques for processing and interpreting seismic data, and was instrumental in developing a micro-seismic device which monitors sonic wave propagation in outcropping geologic structures. In his subsequent position with Garrett Turbine Engine Company, Mr. Rogers conducted rotor dynamics analysis of gas turbine engines and performed 2D and 3D finite element stress and fracture mechanics analyses of engine components, complemented by experimental spin pit tests and focused eddy current programs to monitor crack growth. In addition, he assumed an engine design position and was responsible for the design of variable stator vanes, turbine blades, bearings and seals, as well as bearing vibration monitoring, and drive shaft torsional vibration analysis and monitoring.

Since joining FaAA, Mr. Rogers has directed monitoring, diagnostics and analysis of rotating equipment in industrial, automotive and utility applications, including rotor and structural dynamics, and the development of a state-of-the-art modal balancing code for steam turbine-generator sets.

Mr. Rogers holds a B.S. in Mechanical Engineering from Northern Arizona University and is currently a M.S. candidate at Arizona State University. He is also a registered professional engineer in the State of Arizona.

Clifford H. Wells received advanced degrees in applied mechanics and mechanical engineering from Yale University. He acquired twenty years of experience in structural analysis and mechanics of materials at Pratt & Whitney Aircraft, where he became manager of the mechanical behavior of materials group. He then spent six years in contract research at Southwest Research Institute as Director of Engineering Mechanics and Assistant to the President. He joined Failure Analysis Associates in 1981 as Vice President for Research and Development.

Dr. Wells has authored over thirty technical papers regarding behavior of materials at high temperature and structural integrity, especially of rotating machinery. He is a past president of the Federation of Materials Societies and a fellow of the American Society of Mechanical Engineers.

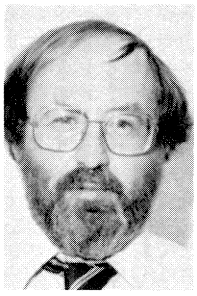

Duane P. Johnson received his B.S. in Electrical Engineering from the University of Minnesota and his Ph.D. in Physics from the University of Washington. He conducted research in applied physics and nondestructive evaluation (NDE) of materials at Pratt & Whitney Aircraft for five years, then he spent four years as a Senior Consultant in NDE and quality assurance at Failure Analysis Associates before forming his own company, Reluxtrol Corporation. This company specialized in the development and application of electromagnetic inspection equipment, and especially in controlled reluctance eddy current generators. He recently rejoined Failure Analysis Associates as manager of NDE and monitoring systems development and field inspection.

Dr. Johnson, author of some fifty technical papers, has contributed significantly to the mathematical basis of inspec-

tion uncertainty and its role in governing structural integrity, as well as the development of advanced flaw detection and sizing procedures.

ABSTRACT

The disks and shafts of large steam turbines are subject to cracking from a variety of causes that may limit the service life of the rotor. These mechanisms include thermal-mechanical (low-cycle) fatigue resulting from startup cycles, creep-rupture from long-term service at elevated temperature, and stress-corrosion cracking in regions of condensation. Cracks may initiate in stress concentration areas such as bores and diaphragm grooves, but in many cases they initiate from pre-existing flaws. Degradation of material, especially temper embrittlement, can combine with crack growth to reduce the remaining service lifetime.

Nondestructive inspection methods and lifetime prediction computer programs have been developed for turbine rotors. The prediction of lifetime requires detailed analysis of potential flaw linkup in regions of high ultrasonic indication density. Transient stress and temperature analysis for the specific turbine duty cycle and rotor geometry, and the calculation of crack growth rates for several possible fracture mechanisms are discussed. The time for a crack to reach critical size is determined by linear elastic fracture mechanics. Illustrations of these analysis procedures and comparisons with actual field service case studies are presented.

INTRODUCTION

The structural integrity of steam turbine rotors continues to occupy the attention of electric utility operators, original equipment manufacturers, insurance underwriters and a growing service industry. The main reasons for this interest are, of course, that the rotor represents a significant safety problem, inasmuch as rotor bursts are not contained within the turbine casing, and an even greater economic risk in view of the long lead time, and thus lost production, involved in procuring a replacement rotor. Concern over the safety of rotors has diminished since the last two reported catastrophic bursts in 1974 and 1977; these incidents are discussed in some detail in this paper. On the contrary, interest in the economics of turbine rotor inspection, repair and replacement has heightened in recent months as the electric utilities have realigned their planning away from construction of new plant capacity and towards the extension of service lifetime beyond the original design lifetime of existing major components. In this context, the primary concern is for the most cost-effective maintenance strategy consistent with an acceptable failure probability, which has been suggested by Bush [1] to be on the order of 3×10^{-4} per year, based upon industry experience.

This paper presents three case studies which demonstrate important mechanisms of rotor failure; i.e., those that have been most prevalent in the electric power industry within the last ten years and that have had the greatest cost impact in terms of inspection, monitoring, analysis, repair and replacement. The turbine rotor is considered to be comprised of an integrally forged shaft and arrangement of disks which carry the blading, or of a shaft onto which disks are shrunk and keyed. Many fatigue and corrosion failures have been experienced by the blading, as well as by stationary parts of the turbines, but these fall outside the scope of this paper. The three problem areas selected for examination are low-cycle fatigue crack growth from the rotor bore hole or from material defects in the near-bore region; stress-corrosion cracking of disks, especially shrunk-on disks of low-pressure turbines; and transverse fatigue cracking of the shafts of low-pressure rotors. Each problem has led to a number of catastrophic or nearly catastrophic failures, resulting in extensive plant outage, and has engendered costly research into new methods of inspection, monitoring and analysis to avoid recurrence. The nature of the cracking mechanism, any symptoms observed prior to failure, the analysis tools presently available and the status of research are discussed for each case.

LOW-CYCLE FATIGUE OF INTEGRAL ROTOR BORES

Concern for the undetected growth of cracks within turbine rotors has led to recommendations for retiring and replacing rotors at great cost to electric utilities. That rotor replacement may be a prudent policy is illustrated by several instances of catastrophic burst, the most recent being that of a 225 MW, tandem compound, triple exhaust 3600 rpm fossil turbine generator [2]. Even more compelling are the numerous, usually undocumented cases of rotors found to contain large flaws or cracks [3]. On the other hand, examples can be cited of rotors that were recommended by the manufacturer for retirement and later were found to have undergone no detectable degradation in service; one such example is documented in reports of the Electric Power Research Institute (EPRI) Research Project RP502, "Integrity of Steam Turbine Rotors" [4]. In many cases, the quality of nondestructive evaluation data, combined with uncertainties in material properties and power plant duty cycles, has not permitted an accurate analysis of burst margin or remaining life, and the electric utility or its insurance underwriter has been obliged to follow the recommendations of the manufacturer.

Nature of Bore Cracks

Near-bore cracks in most rotors originate in either the forging or heat-treating process, or grow from pores and inclusions present in the ingot that were not "healed" or dispersed adequately by forging. However, near the inlet stages of high-pressure and reheat turbines, where metal temperatures may exceed 900°F, cracks also may develop at the bore surface in the absence of manufacturing flaws, as a result of the combined effects of stress-rupture and low-cycle fatigue. Manufacturing-induced flaws tend to be concentrated in bands of compositional segregation or at the central "pipe" of the ingot. The segregation results from convection of liquid metal during solidification and generally follows the liquid-solid interface at an angle to the ingot centerline, while the pipe results from shrinkage near the ingot centerline that is last to solidify. Forging may effect solid-state bonding of clean porosity materials and may break up and disperse nonmetallic inclusions. Because the forging reduction is less near the rotor centerline, it has been the usual practice in the U.S. to remove the porous material by boring. However, certain European manufacturers prefer not to bore the rotor, because critical crack sizes in an unbored rotor are ten times larger than the critical size of a bore-surface connected crack.

The three mechanisms that need to be considered in understanding the nature of bore cracks are brittle fracture, subcritical crack growth and flaw linkup. These are briefly discussed below.

Brittle Fracture

Regardless of flaw type (inclusions, etc.), material fracture takes place by crack growth and linkup under the tangential (hoop) stress resulting from thermal gradients and centrifugal loading. Therefore, the most important flaw characteristic to measure is its maximum axial and radial extent. Catastrophic fracture is known to occur when the crack-tip stress intensity

factor (K), which is proportional to the local tangential stress and the square root of the crack depth, equals the fracture toughness of the material. The fracture toughness, as shown in Figure 1, varies significantly with temperature; therefore, it is necessary to know both the local stress and temperature histories in order to calculate the largest crack which will *not* grow.

Also, large differences in fracture toughness are observed both between as-manufactured rotors and between hot and cold sections of a single rotor after prolonged service exposure. Unfortunately, no nondestructive means of predicting fracture toughness is available, and recourse must be made to Charpy impact or fracture mechanics tests.

Subcritical Crack Growth

Calculation of the remaining lifetime of a rotor can be performed to determine the number of starts required for a crack to grow from its current size to the critical size. For isolated flaws these calculations are simple: they involve merely integrating published or experimentally determined crack

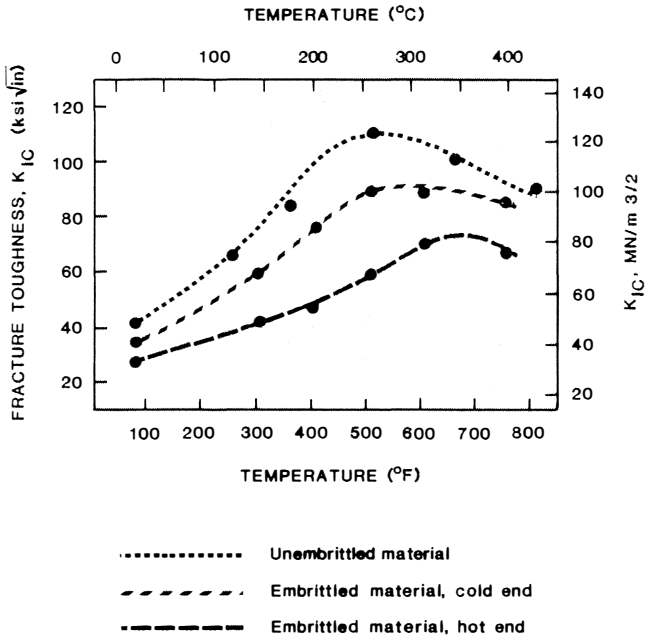

Figure 1. Effect of Temper Embrittlement on Fracture Toughness of 1CrMoV Rotor Steel.

growth rate data, such as those shown in Figure 2. As is the case with fracture toughness, crack growth rate varies with temperature and degree of embrittlement; in addition, growth rates at elevated temperature are frequency dependent. A single parameter can be employed to represent effects of both temperature and frequency on fatigue crack growth rate. However, there are a few situations in which crack growth may occur under steady-state stress at high temperature; i.e., under creep rupture conditions. Creep crack growth rate data are conventionally correlated on the basis of a "path-independent crack-tip integral" of strain energy dissipation rate (C*) [5]. Figure 3 shows the compilation of some available data.

Linkup of Clustered Flaws

Rotor forgings are inherently "dirty" and contain a large number of small inclusions and pores that scatter ultrasound back to the transducer. In general, there is no reason to be concerned about an isolated flaw of less than ⅛ inch diameter, even in the most critically stressed rotor; this acceptable size increases significantly with distance from the bore. However, in the case of multiple flaws that are closely spaced, critical linkup between clustered flaws must be considered. In general, the ligaments between small flaws will yield before the critical stress intensity level is reached. Figure 4 illustrates this limitation for an idealized situation with equally spaced cracks of the same size, aligned in a row perpendicular to the tangential stress.

Unfortunately, inclusions and pores are not neatly aligned as in Figure 4, but are randomly dispersed throughout the volume of the rotor. Since cracks propagate under the tangential stress, we are primarily concerned about flaws that can link up in the radial and axial directions. A conservative procedure to allow rapid sorting of ultrasonic indications has been developed. The technique involves geometric grouping of flaws and approximation of elliptical cracks with conservative constraints. Reference 4 describes this technique in detail.

Case Study 1: 225 MW IP Rotor Burst [2]

The 225 MW IP rotor fractured from two large cracks,

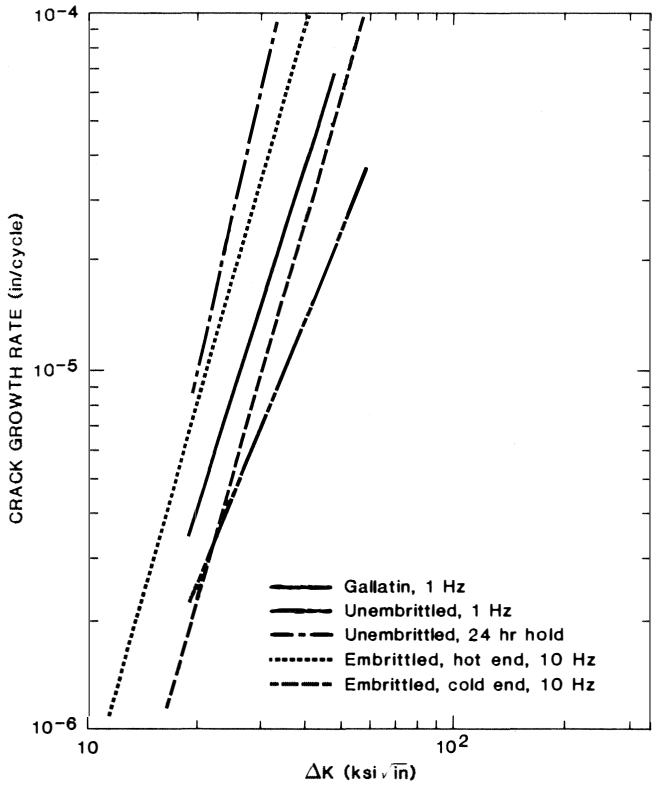

Figure 2. Crack Growth Rate Data.

located approximately 180° apart, both with the size and shape indicated in Figure 5. The initial diagnosis of the failure mechanism as a creep-fatigue interaction has been presented in Reference 2, which describes the operating history, material properties and other factors. The rotor forging had been given a production ultrasonic examination but had not been examined from the bore surface. Further analysis tended to discount the role of creep and implied the existence of near-bore cracks of critical size early in the life of the rotor, since the number of fatigue cycles was only approximately 200. The two large cracks were concluded to be dynamic cracks that had stopped.

The origins of these cracks were found to be in stringers of manganese sulfide inclusions in regions of dendritic segregation. The origins, the larger of which was approximately 5.5

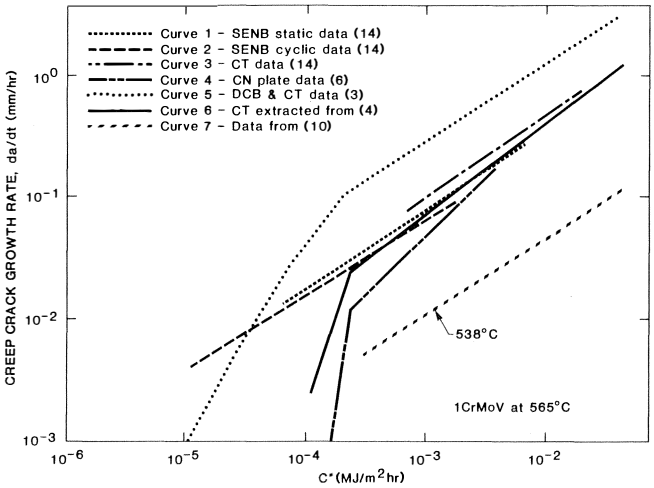

Figure 3. Summary of Correlations Based on the Parameter C.*

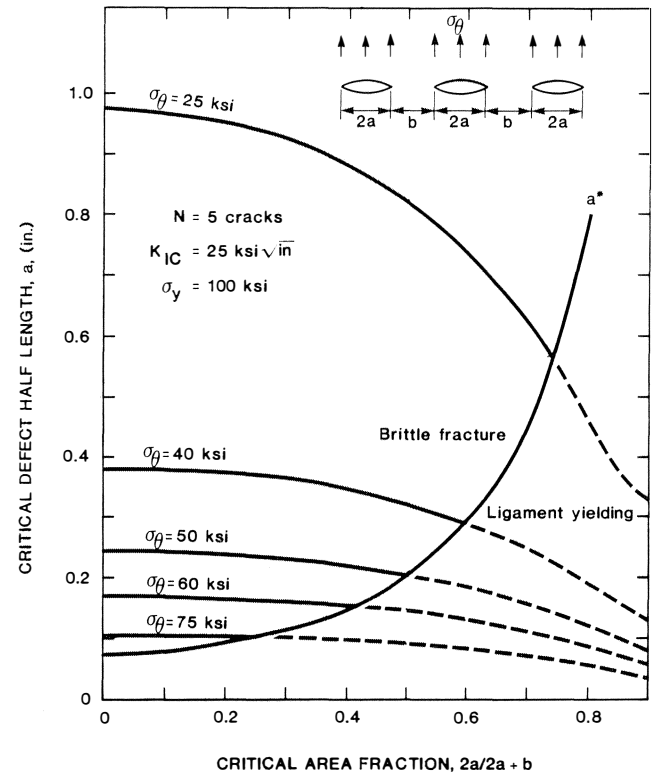

Figure 4. Limits of Fracture Mechanics in Predicting Cracking Within Clusters.

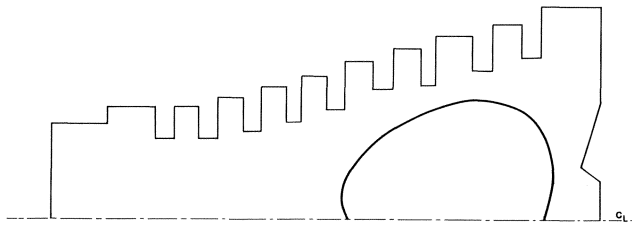

Figure 5. 225 MW IP Rotor Crack.

inches in axial length by 0.3 inch in radial extent, exhibited intergranular fracture which could be reproduced in a room temperature impact or tube burst test in material from the vicinity of the fracture. The size and location of the larger origin was consistent with the measured fracture toughness and calculated stress-temperature history for a cold start. No definite evidence of subcritical crack growth could be found. It was concluded that the origins could have been detected and sized by present-day bore ultrasonic examination procedures.

Some controversy exists over the possibility of monitoring the growth of large, radial-axial cracks of the type found in the subject rotor. Plant records show difficulty in maintaining balance of the unit over much of its life, and significant changes in vibration phase and in sensitivity to temperature increases were assumed to coincide with the development of one or both of the large cracks. Finite element calculations of the mode shapes and frequencies of the rotor were carried out at the Georgia Institute of Technology for various crack configurations, and no significant effect of the radial-axial cracks could be determined on the lateral vibration response of the rotor, except at very high frequencies [6]. This result was rationalized on the basis that the transverse shear stresses acting on the plane of the crack were very low. No torsional response calculations were made. The possibility exists of an eccentricity developing through the opening displacement of a single crack under centrifugal and thermal tangential stress.

Bore Crack Analysis Lifetime Prediction

Flaw Characterization

To help understand the nature of the 225 MW IP rotor failure, five retired 1 Cr-Mo-V rotors were dissected, including

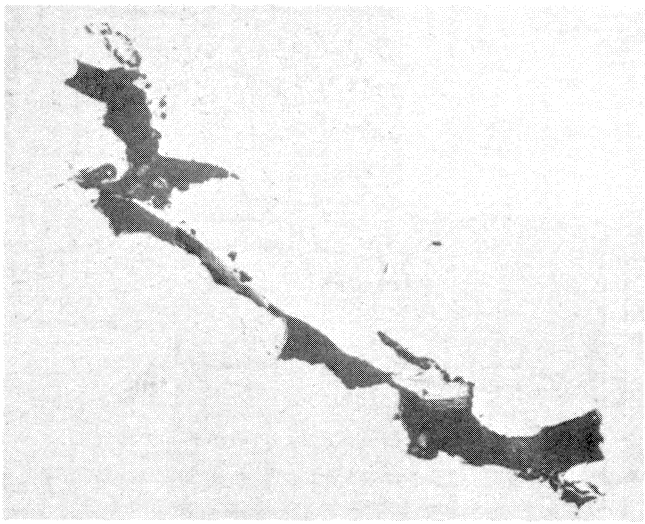

Figure 6. Typical Flaw in a Different IP Rotor Revealed by Sectioning. Magnification = 100×.

one which had developed a crack 4 inches deep by 16 inches long. The most significant characteristic was irregularity of the boundaries, which probably is beneficial from the standpoint of scattering ultrasound.

Figure 6 illustrates a flaw that is typical of those found in two of the rotors and is essentially a partially closed gas or shrinkage pore with associated forging laps and small MnS inclusions. Figure 7 shows a section through a large holding indication in an IP rotor donated to the RP502 project. This flaw was the basis of a recommendation by the manufacturer to retire the rotor. The flaw has slag-like inclusions and some MnS particles comprising the dark branches, which are surrounded by a relatively dark etching region, indicating chemical segregation. It is thought that this region was initially connected to the central pipe and that it represents shrinkage that was filled with slag before forging. Certain areas appear to

be crack-like; however, there is no evidence of any service-induced cracking associated with this flaw.

The most difficult flaw to measure ultrasonically is generally conceded to be a tight fatigue crack precisely oriented in a radial-axial plane. This flaw would be typical of bore-connected, elevated temperature thermal fatigue cracks. Figure 8 indicates the satisfactory agreement between inspection results and destructive evaluation of an intergranular crack in a test block. The inspection was performed by an EPRI-developed, immersion, focused shear beam ultrasonic system known by the acronym TREES.

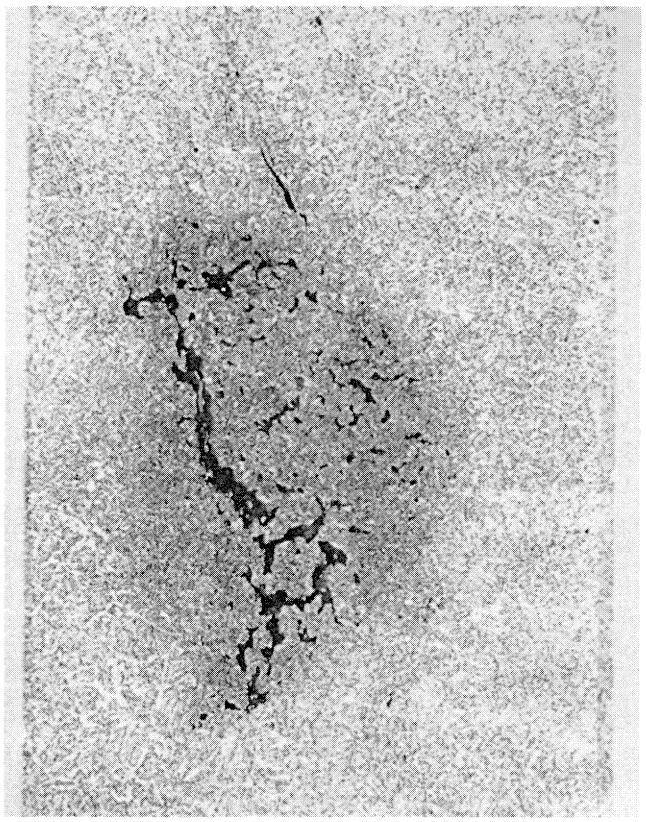

Figure 7. Radial-Tangential Section Through Holding Indication in IP Rotor. Stress Axis Is Horizontal. Nital Etch. Magnification = 20×.

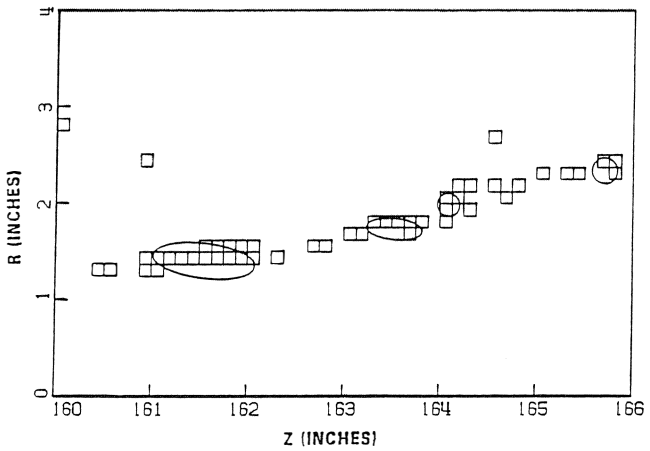

Figure 8. Holding Indication in Rotor—TREES Cell Data and FRAC Linkup Prediction (SAFER Results). Source: Southwest Research Institute.

The SAFER Automated Lifetime Prediction System

Under EPRI sponsorship, a computer program was developed to allow the prediction of remaining lifetime of rotors from the results of bore ultrasonic examination and duty cycle history. The current version of this code, known as SAFER (for Stress and Fracture Evaluation of Rotors), is undergoing verification at the EPRI NDE Center in Charlotte, North Carolina. Figure 9 shows the overall flow diagram for the analysis. A probabilistic lifetime prediction program is also under development. In lieu of a proven method of monitoring turbine rotors for radial-axial cracks, bore inspection, combined with the SAFER code, represents the major insurance against rotor burst directly available to the utility operator.

DISK CRACKS

Disk cracking occurs primarily in wet steam environments and is normally attributed to stress corrosion cracking (SCC). Cracking has been observed in turbines produced by all three

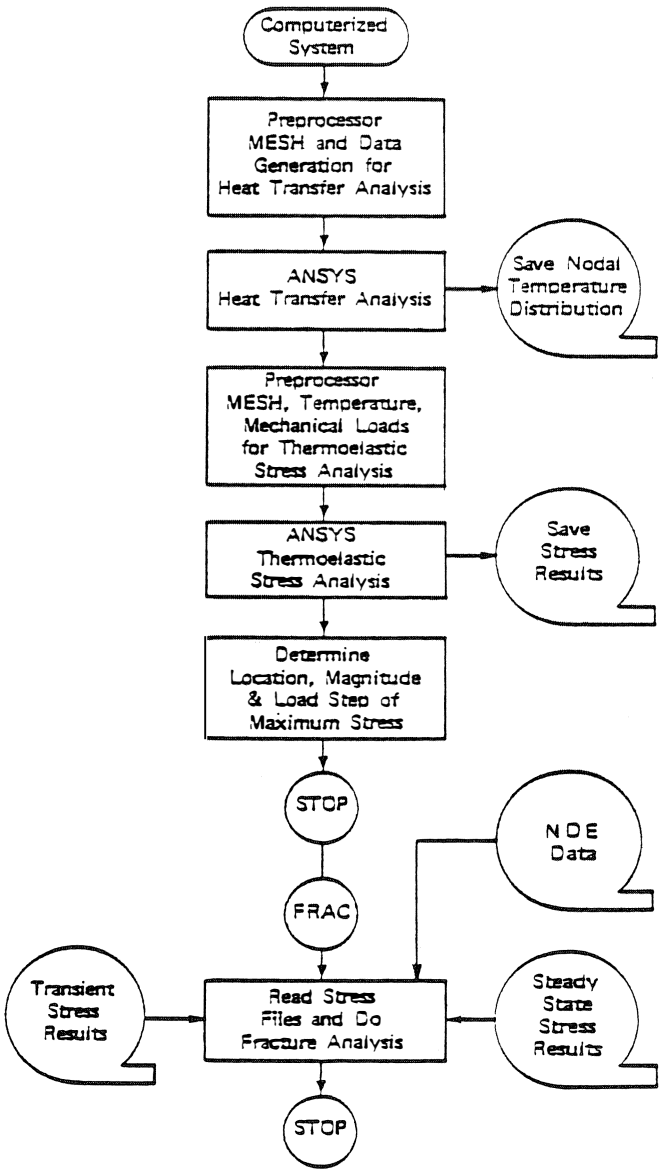

Figure 9. Flow Diagram for the Current Version of SAFER.

U.S. manufacturers and in all three major disk steels (2.5 Ni-Cr-Mo-V, 3.5 Ni-Cr-Mo-V, and 1 Cr-Mo-V).

Nature of Disk Cracks

Disk cracking occurs at keyways, bores, rim-blade attachments and web faces. According to an EPRI report [7], there have been over 70 cracked disks observed in U.S. nuclear fueled electric generating stations and 50 cracked disks observed in U.S. fossil fueled electric generating stations over the last few years. The distribution of cracks is summarized below.

Crack Location	No. of Disks
Rim–Attachment	46
Web-Face	38
Keyway	36
Bore	6

A detailed failure analysis of one such disk, which failed from a stress-corrosion crack initiating in the blade attachment area, is presented below [8]. The investigation was directed toward establishing the cause of failure and estimating the reliability associated with continued operation, repair, and replacement options for the failed rotor and similar units. During the investigation, it became evident that conventional magnetic particle tests do not reliably detect SCC. A critical area eddy current inspection that has a much higher detection reliability for SCC was developed.

Case Study 2: 130 MW LP Disk Burst [8]

On August 21, 1977, 1 hour and 13 minutes after the unit was started following a maintenance shutdown, a last stage low-pressure turbine disk ruptured on a unit owned by a northeastern electric utility. The turbine was rotating at its 1800 rpm operating speed when the rupture occurred. The unit was a cross-compound, eight stage, double-flow turbine rated at 130 MW and had operated for 23 years prior to failure. A typical cross section of the turbine is shown in Figure 10.

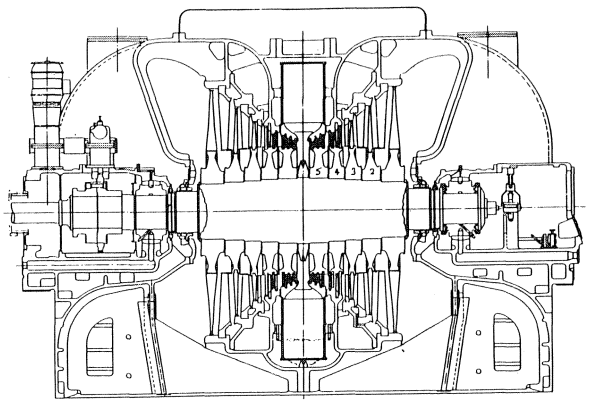

Figure 10. Typical Cross Section Through LP Turbine of Close-Coupled, Cross-Compound, Reheat Unit.

The last stage disk had an 80 inch OD and a 36 inch ID, and it was 17.5 inches wide at the bore. The disk fractured into two major pieces, accompanied by a number of smaller fragments. Figure 11 is a sketch of the fractured disk, with the recovered pieces labeled and the crack progression indicated.

The physical distortion of major pieces and the macroscopic markings on the fracture surface indicate the following failure sequence. The initial cracking started near piece B-12A

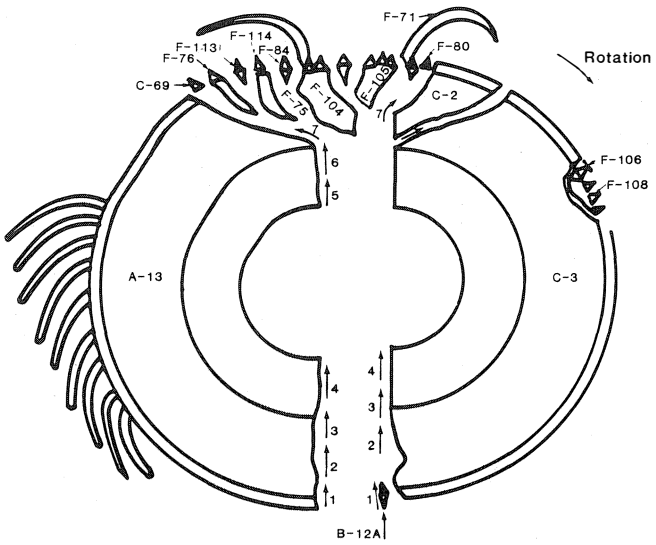

Figure 11. Sketch of the Fractured Disk Labeling the Pieces Recovered and Indicating the Crack Progression.

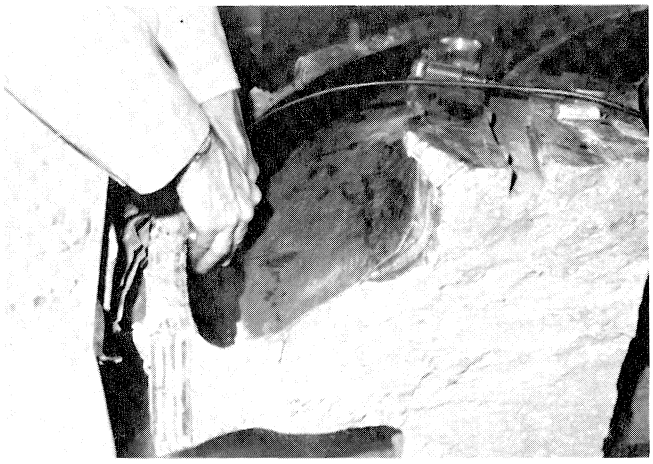

Figure 12. View of the Primary Fracture Origin Area on Piece A-13.

(at Point 1 of Figure 11) and propagated radially inward (Points 1-4) to the bore. Figure 12 shows a view of the fracture surface on piece A-13. Once it had fractured through, centrifugal force caused piece A-13 to pull away from the shaft and distort (bend), primarily at the other end of piece A-13. As piece A-13 lifted away and bent, the stresses at the bore (Point 5 of Figure 11) increased and initiated a brittle cleavage crack, which split to produce the many small pieces (e.g., F-75, F-104, F-105, C-2).

Piece A-13 exited the turbine casing with a trajectory sloping upwards at about 15 degrees. Exiting the building, the segment sheared through a 12 inch steel beam and perforated a 6 inch thick reinforced concrete wall. The segment then struck a 55,000 lb transformer, whose end was displaced about 6 feet, deflecting the segment's trajectory slightly to one side. The segment then bounded off the side of an adjacent hill and impacted equipment in the switchyard on top of the hill. The segment came to rest 355 feet away from and 60 feet above the turbine axis.

Piece C-3 separated from the shaft on a slightly downward trajectory, producing extensive damage to structural members in the lower turbine casing and to the edge of a massive concrete wall that forms a part of the foundation. The segment

ricocheted up from this area, denting the side of the cowling on the adjacent IP turbine, damaging the insulation on piping beneath the cowling and producing a 3 foot deep dent in a steel beam in the wall of the building before coming to rest on the floor.

Fractography

The primary fracture surface is shown in Figures 13 and 14. The crack initiated on the rim slot approximately 0.15 inch in from the inlet face. In the subcritical crack growth region, the fracture was primarily transgranular quasi-cleavage, with some interspersed intergranular fractures. The critical crack size appeared to be nearly a quarter-elliptical corner crack of radial depth 0.15 to 0.20 inch and surface length along the groove of 0.60 inch.

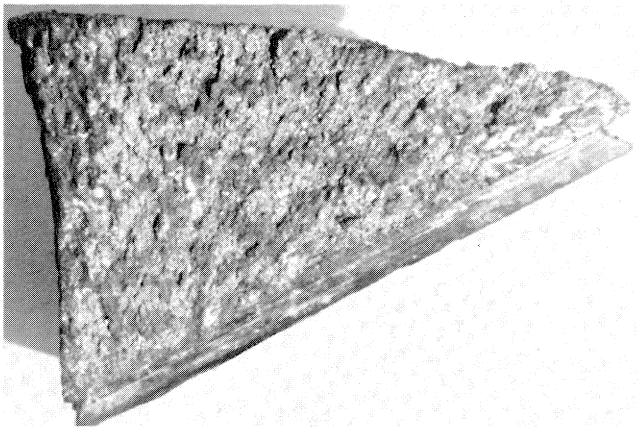

Figure 13. Photograph of Primary Fracture Side of Turbine Disk Fragment. The Machined Surface at Bottom of Figure is Bottom of Rim Slot. The Balance of the Inlet Face of Disk Is at Left. Disk Steeple Has Been Cut Off as Shown in Figure 14.

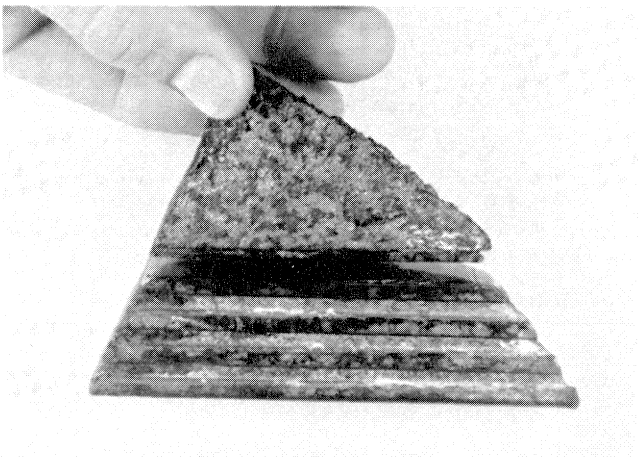

Figure 14. Relationship of Fracture and Fir Tree.

Metallography and Chemical Analysis

Figure 15 is a metallographic section through the primary fracture origin and parallel to the inlet face of the disk. The primary fracture surface is along the top, with a portion of the rim slot in the upper left-hand corner. The secondary fracture surface is running diagonally from upper right to lower left.

The microstructure was relatively coarse and bainitic, with no observed microstructural inconsistency at the fracture origin. Some corrosion pitting and secondary cracking at the grain boundaries were observed just below the fracture surface, at the machined surface. Evidence of cold work, extending approximately 0.001 inch into the material, was visible on the machined surface.

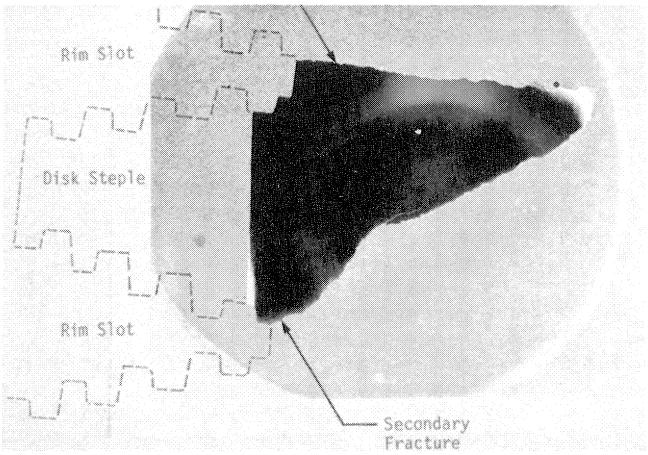

Figure 15. Metallographic Specimen Through Primary Fracture Origin and Parallel to Inlet Face of Disk. Primary Fracture Surface Is Along Top With Portion of Rim Slot in Upper Lefthand Corner. Left Edge of Specimen Is the Result of Cut to Remove Fir Tree. The Lower Edge of the Specimen Is the Result of a Secondary Fracture from Adjacent Rim Slot. (Approximately 1.5×).

Nondestructive inspection of the other rim slots in the failed disk revealed other crack indications. Several of these indications were metallographically examined by progressively polishing parallel to the disk face. Perpendicular to the plane of the crack, the characteristics of each crack varied considerably along its length, as shown in Figure 16. At some locations the crack was very wide and contained some corrosion product, while at other locations it was very tightly closed and barely visible in the micrographs. Some crack branching was observed, and in some planes the crack appeared to be discontinuous. In general, the crack path appeared to be independent of the microstructure, although some of the branching appeared to be along bainite packet boundaries.

Extensive chemical analysis of the deposits found in steeple grooves was conducted. Noteworthy observations were that sulfur was more prevalent in the failed disk than in the unfailed disk, particularly at the inlet face near the primary fracture, and that a significant amount of sulfur was present within the small secondary cracks.

Nondestructive Inspections

During destructive examination of the failed disk, small surface-connected secondary cracks were detected in other fillet radii. Careful magnetic particle inspections in the laboratory were then used to locate other secondary cracks. The conventional magnetic particle inspections did not reliably detect the small cracks that would be of concern under field inspection conditions. Therefore, an improved inspection procedure was required to assess the condition of the remaining disks in operation. To accomplish this goal, an improved magnetic particle (MP) technique and a focused field eddy current inspection procedure were developed in parallel.

Table 1 summarizes the results of the magnetic particle inspection and the focused field eddy current inspection. The improved (2500 AMP) magnetic particle tests were able to detect the crack in dovetail 4-2 and showed possible cracks in dovetails 4-1 and 5-2. No crack indications were observed in dovetail slot 11-1 and 11-2. The eddy current inspection using

Figure 16. Etched, Metallographic Cross Section of a Secondary Crack Found by Nondestructive Inspection in Rim Slot Number 4. Note Variation in Width of Crack. (50×, left; 100×, right).

a 3 mm detection threshold indicated that dovetail slots 4-1, 4-2, 5-2, 11-1, and 11-2 definitely were cracked. Metallographic sectioning of the dovetail slots indicated that all the slots identified by the eddy current tests were indeed cracked. Figure 17 shows the crack in dovetail 4-1, and Figure 18 shows the crack in dovetail 4-2. Figure 19 shows the crack in 11-1 that was missed by the magnetic particle tests. It is evident that the magnetic particle test is only able to detect the larger open cracks, while the eddy current test is able to detect much smaller and tighter cracks.

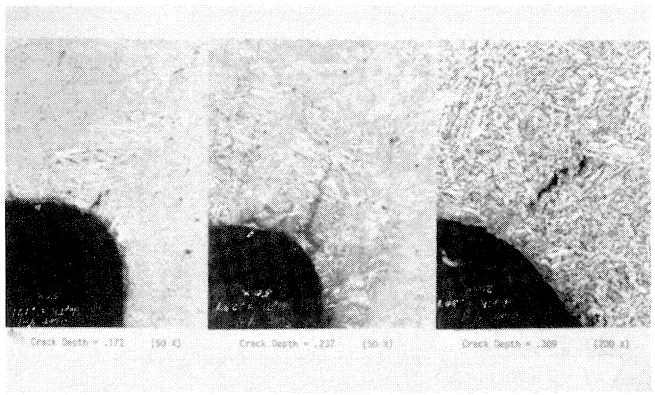

Figure 17. Dovetail Slot 4-1 at Various Depths Below the Inlet Surface. Nital Etch.

Stress Analysis

To provide a design comparison and to assess the possibility of similar failures in the other three units (No. 1, No. 2, and No. 4) at the generating station, stress levels were calculated for all four disk geometries. Concentrated stress levels in the fillet radii of the last stage disks on all four units were calculated, both with the nominal 0.025 inch radius fillet and for a proposed remachined 0.05 inch radius fillet. Units No. 2 and No. 3 had nominally identical concentrated stress levels, while

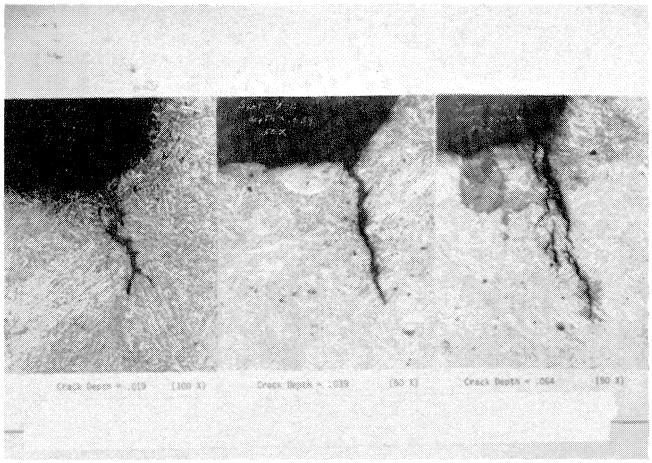

Figure 18. Dovetail Slot 4-2 at Various Depths Below the Inlet Surface. Nital Etch.

Table 1. Magnetic Particle Indications Obtained from Primary Fracture Piece No. C3-3.

Dovetail	Yoke	600 AMP	900 AMP	1400 AMP	2500 AMP	Residual
4-1	-	-	-	-	VL 0.1	VL 0.1
4-2	L 0.2	L 0.2	L 0.35	L 0.35	M 0.4	M 0.4
5-2	VL 0.2	-	-	-	VL 0.1	VL 0.1
11-1	-	-	-	-	-	-
11-2	-	-	-	-	-	-

Eddy Current Indications Obtained from Primary Fracture Piece No. C3-3.

	Detection Threshold				
Dovetail	8 mm	6 mm	4 mm	3 mm	2mm
4-1	0.1	0.2	0.3	0.3	0.3
4-2	0.1	0.2	0.2	0.2	0.2
5-2	0.02	0.05	0.05	0.15	0.15
11-1	-	-	0.1	0.2	0.2
11-2	-	0.1	0.2	0.4	0.5

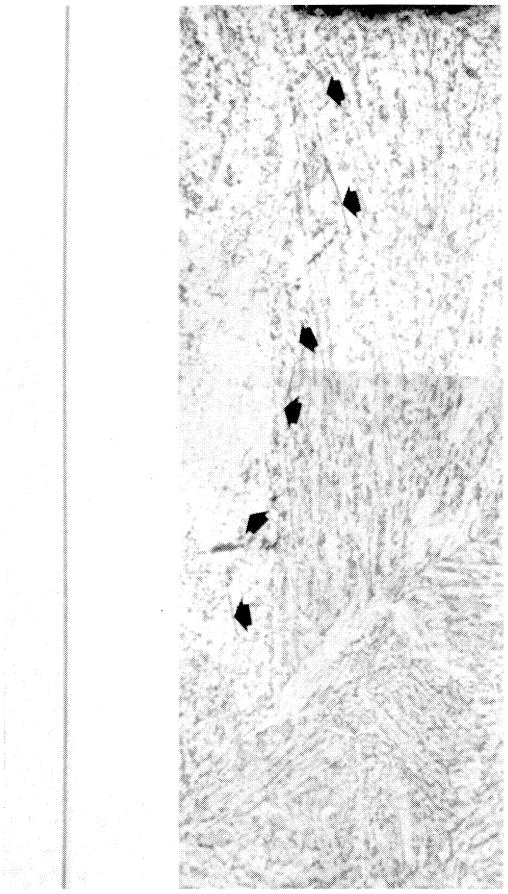

Figure 19. Crack in Groove 11-1 at 0.202 in. Magnification = 250×.

No. 1 and No. 4 had lower concentrated stress levels due to a reduced bore-shaft interference fit in these units. Even without the imposition of thermal gradients (which could increase all stress levels by as much as 25%), the concentrated elastic stress computed in the 0.025 inch fillets of Units No. 2 and No. 3 was 157 ksi. Remachining the fillet radius to 0.050 inch would reduce the stress in the No. 2 and No. 3 disks to 116 ksi. The calculated concentrated stress for the Unit No. 4 disk with a 0.05 inch radius fillet was 100 ksi.

Materials Testing

The major objectives of the materials testing program were to quantify how the times to crack initiation and failure are affected by different loadings and environments, and to quantify any differences in susceptibility to H_2S SCC that may exist among the four unit materials. The H_2S-saturated water environment was selected for the bulk of this investigation because initial screening tests showed that H_2S solutions were the only candidate solutions which produced an SCC mode similar to the primary crack which caused the disk failure, and because it represented an extreme but realistic environment for generating SCC in reasonable test time.

Other conclusions drawn from the material testing program were that dwell time at load is the major contributor to crack initiation and failure in H_2S-saturated water, but that fatigue loading, representing start-up and shutdown, has a minor effect. Disk materials in Units No. 1 and No. 4 had greater crack initiation and propagation resistance than those used in the other two units. Standard Charpy specimens of disk materials showed that the crack initiation lifetime was four times better for No. 4 than No. 3, and that the same material had a crack growth rate, on the average, four times slower than that of the Unit No. 3 material in H_2S-saturated water at high K levels. Finally, the stress dependence on crack initiation time for both of these materials was found to depend upon the stress to the fourth power.

Fracture Mechanics and Reliability Analysis

Two types of fracture mechanics calculations were performed. The first was directed at comparing the primary fracture stress intensity factors with the measured material toughness values. The second was directed at a "relative" life prediction for the failed and unfailed disks with the various repair options. These relative life calculations were then combined with failure rates, as implied by the failure of 130 MW Unit No. 3 and the successful operation of similar units, to develop a failure probability and expected failure cost for the various units and repair options [9].

Excellent agreement was found between the measured and computed critical crack sizes for the failed LP disk. This agreement supports the accuracy of the stress and fracture mechanics analysis.

The estimated SCC failure rates for the three remaining turbine units are presented in Table 2, along with the average failure rate for the entire turbine generator industry [1]. Because of the lower steady stresses and the greater material resistance to sulfide SCC, Units No. 1 and No. 4 had a significantly lower failure probability than No. 2 and No. 3, and they had an estimated failure rate only slightly above the industry average. By increasing the fillet radius to 0.050 inch, the concentrated stress would have been further reduced, and, correspondingly, the estimated failure rate would have been reduced to well below the industry average. Figure 20 summarizes the failure rates and expected failure costs associated with the various units.

Turbine operators now have access to a focused field eddy current inspection technology, which could have detected at a very early stage the crack which led to the failure of Unit No. 3.

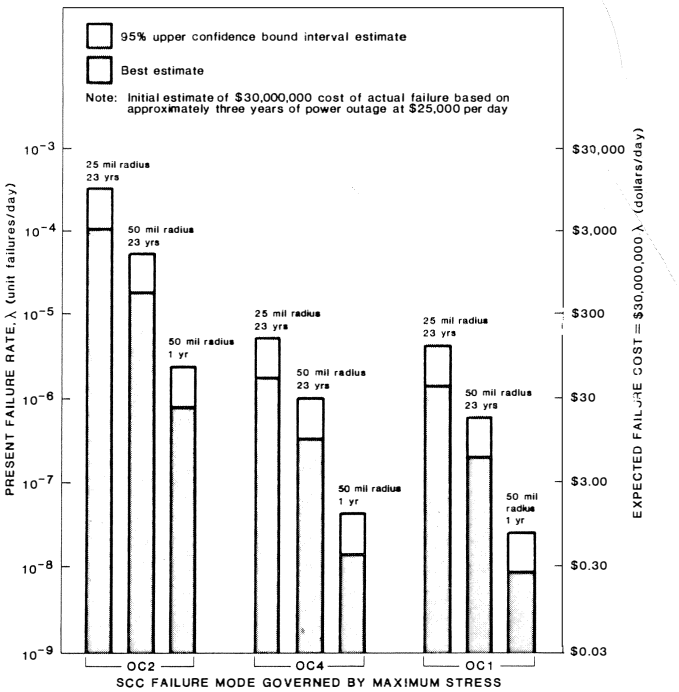

Figure 20. Estimates of Daily Failure Rates and Expected Costs for Exhaust Disk Rim Cracking Failure Mode in a Northeastern Utility's Units No. 1, No. 2, and No. 4.

Table 2. Best Estimates of Failure Rates for Turbine Units No. 1, No. 2, and No. 4.*

FAILURE MODE GOVERNED BY MAXIMUM STRESS (Stress Corrosion Cracking Failure Mode)				
UNIT	NOMINAL FILLET RADIUS (mils)	EFFECTIVE** AGE, t_a, OF MATERIAL EXPOSED BY MACHINING (yrs)	FAILURE PROBABILITY PER DAY	RATIO OF OC2 (25 mil radius) FAILURE RATE TO CALCULATED FAILURE RATE
No. 2	25	N/A (23)	113×10^{-6}	≡1
	50	23	19.5×10^{-6}	6
	50	1	0.84×10^{-6}	135
No. 4	25	N/A (23)	1.85×10^{-6}	61
	50	23	0.35×10^{-6}	320
	50	1	0.015×10^{-6}	7,500
No. 1	25	N/A (23)	1.04×10^{-6}	109
	50	23	0.21×10^{-6}	540
	50	1	0.0091×10^{-6}	12,400
Turbine Generator Industry Average			$.9\times10^{-6}$	125

*Standard structural techniques were also applied to obtain confidence interval estimates of the failure rates to account for sampling errors introduced by the fact that only one field failure has occurred. In general, the 95% (upper) confidence interval estimates are approximately three times larger than the best-estimate failure rates, and the 5% (lower) confidence failure rates are approximately twenty times smaller than the best-estimate values. Our estimates of the relative failure probabilities of the units are not affected when made on a confidence interval basis.

**Since new surfaces would be exposed by machining the 25 mil fillet radius to 50 mils, it might be argued that the actual age, t_a, of the new, presumably crack free, material is smaller than 23 years. However, a counter argument is that the material on the side (radial circumferential plane) of the disk is still the old surface and should be regarded as 23 years old. To bound this modeling uncertainty, we have made failure probability and cost estimates for two assumed values, t_a = 1 year, and t_a = 23 years, for the 50 mil geometry.

Also, combined analysis codes are currently available for quantitative assessment of failure rates under a variety of conditions.

ROTOR SHAFT TRANSVERSE CRACKS

Within the last few years, the U.S. utility industry has been experiencing an increase in the initiation and propagation of transverse cracks in large steam turbine rotors. The occurrence does not necessarily appear to be manufacturer-specific and may be a result of changes in unit operational requirements which produce stress conditions, both transient and steady state, that exceed design limits.

Nature of Transverse Cracks

Transverse cracks that initiate on the outside surface of a rotor shaft and propagate through the cross section may be divided into two categories. The first is typified by circumferential-radial cracks initiated and propagated by high axial thermal stresses in the region of a diametral section change, such as a diaphragm groove fillet radius. Thermal transient cycles can initiate several circumferentially spaced crack origins, which may grow together to produce a completely circumferential-radial transverse crack (see Figure 21). Cracks of this type propagate under thermally induced low-cycle fatigue (LCF) until they become large enough that increased driving forces cause the ultimate failure due to high frequency rotational bending loads.

The second type of transverse crack is characterized by a more local initiation site, such as the keyway of a shrunk-on disk. Crack propagation is by high frequency fatigue (HFF) due to rotating bending, though growth occurs under transient thermal conditions where the near-surface mean stress is increased (see Figure 22). The crack initiation process may be LCF-induced through a combination of thermal/mechanical

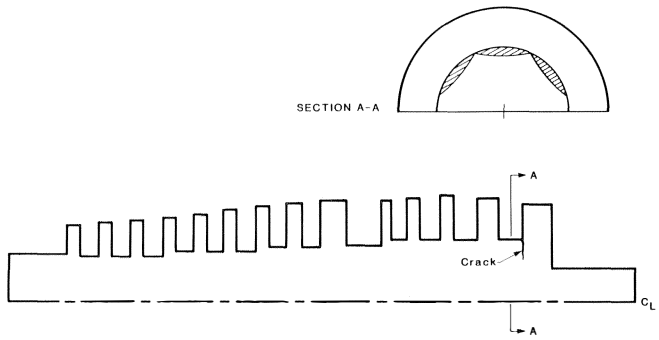

Figure 21. Transverse Crack Initiating at a Filler Radius Diaphragm Groove.

stresses (i.e., shrink fit, start-up, coast-down, or steam temperature changes) or may be the same HFF mechanism used to propagate the crack. This local propagation typically produces asymmetric changes in rotor bending stiffness, whereas the first crack example may produce axisymmetric reduction in effective shaft stiffness. Both crack types should be considered when assessing the effectiveness of crack detection monitoring techniques.

In turbine applications where the rotor is subjected to high steam temperature (i.e., HP or IP inlet stages), there is some evidence of reduction of the material's resistance to crack growth with time [10]. This high temperature exposure can cause temper embrittlement of low-alloy steels and subsequent increase of fatigue crack growth rates. Therefore, it is possible that, due to material degradation, a transverse crack may grow slowly under LCF, but ultimately fail in HFF well before normal fracture mechanics analyses would predict.

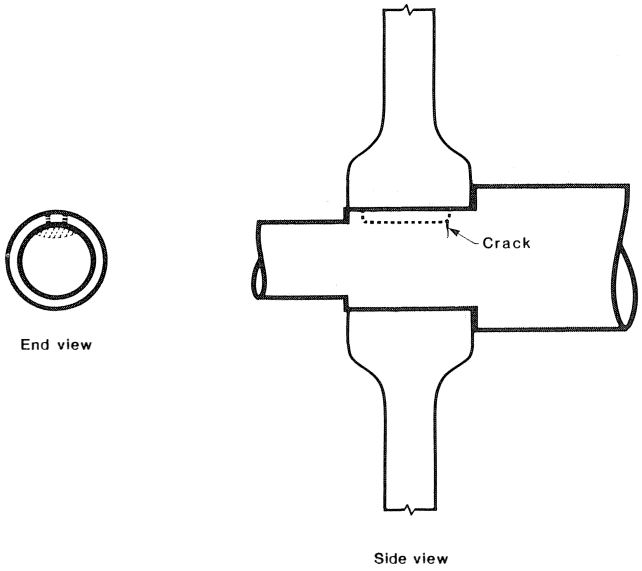

Figure 22. Transverse Crack Initiating From a Keyway.

Case Study 3: 320 MW Double Flow LP Rotor Tranverse Shaft Crack

A northern utility reported abnormal transient vibration levels during boiler deslagging operations associated with a 320 MW steam turbine generator. Of particular interest were the vibration levels recorded at the main bearing caps of the low-pressure, 1800 rpm turbine generator set.

Boiler deslagging was performed on this unit to dislodge slag that accumulated on the outside walls of water and steam tubes. The procedure calls for reduction in furnace firing rates, which causes cooling in particular tube regions. Subsequent thermal contraction effectively dislodges mineral deposits.

The vibration characteristics of the bearing caps during full load, steady state operation were found to be essentially the same as those recorded during early stages of unit operation. Horizontal, vertical, and axial vibrations were recorded for each bearing cap. Also, shaft rider sensors monitored vibration at an angle of approximately 25° from vertical. In addition to variation in transient vibration level, the utility had reported a higher frequency of alignment corrections being required as the rotor aged.

Vibration Analysis

Figure 23a is the normal steady state vibration signature obtained with a shaft rider probe at the No. 1 turbine bearing. A strong, synchronous 1800 rpm signal and very slight two- and three-per-revolution signals are present. Figure 23b, on the other hand, shows the signature at peak vibration levels subsequent to a thermal down ramp of 140°F (77°C). Note the increase in the one-, two-, and three-per-revolution amplitudes.

The vibration characteristics of turbine bearings No. 1 and No. 2 were very similar, and a comparison of vibration data and other parameters indicated a correlation between steam temperature and vibration amplitude. It was observed that a decrease in steam temperature resulted in a vibration level increase. Increases in steam temperature, on the other hand, either did not affect the vibration or reversed a vibration increase associated with a previous temperature decrease. As expected with thermally induced phenomena, there was a definite time lag between steam temperature change and the observed change in vibration.

An example of the vibrational response associated with steam temperature variation is shown in Figure 24. Reduction

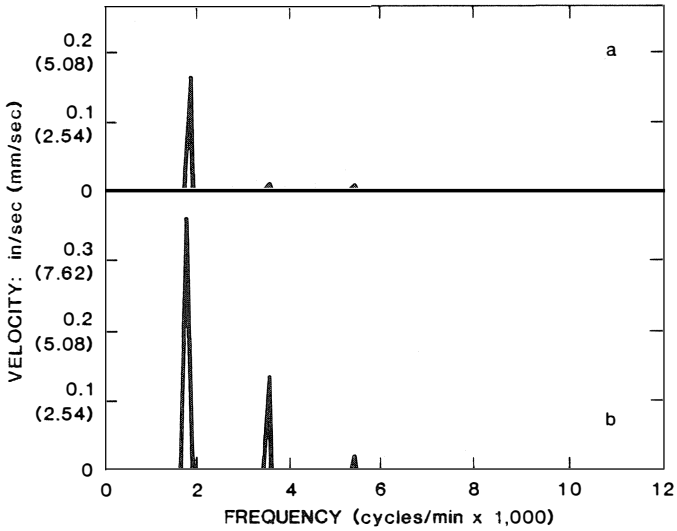

Figure 23. Shaft Rider Vibration Signature of Amplitude vs. Frequency, a) During Normal, Fill-Load Operation, b) During Peak Vibration Subsequent to a Thermal Down Ramp.

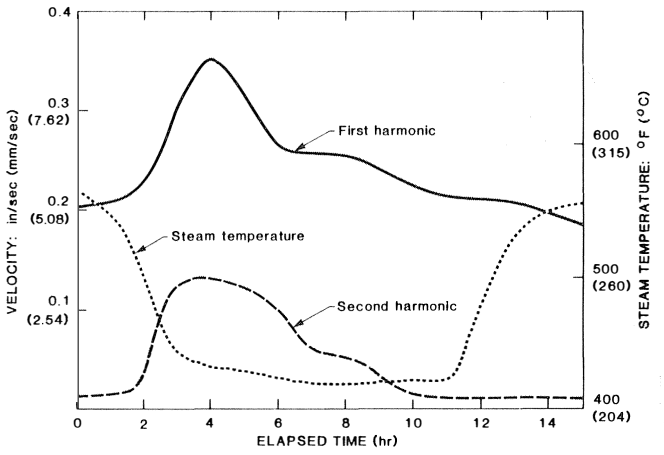

Figure 24. Vibration Amplitude of First and Second Harmonic and Inlet Steam Temperature vs. Time.

in steam temperature cools the surface of the shaft relative to the shaft bore. This condition produces tensile hoop stresses and tensile axial stresses of such a magnitude that a transverse crack in the shaft near the surface would open.

Vibration Response of a Shaft Containing a Transverse Crack

The cause of abnormal transient vibrations was concluded to be a transverse rotor shaft crack located somewhere near the center of the rotor. Several researchers [11, 12, 13, 14, 15] have shown that a continuously open transverse crack produces a twice-per-revolution rotor response due to a linear asymmetrical stiffness analogous to an elliptical shaft geometry. An opening and closing (breathing) transverse crack, on the other hand, may produce synchronous, two, three, or even higher multiples of synchronous response due to the form of the orbit. A completely circumferential crack, however, reduces shaft stiffness and will not excite multiple or subsynchronous rotor response, but instead may reduce the apparent critical speed, depending on crack position. Unfortunately, the crack must grow quite large to substantially reduce the stiffness.

The nature of the crack and the state of stress associated with the deslagging thermal transients previously described suggest that the crack was primarily open during the periods of

high vibrational response, with some cyclic loading due to rotating bending. Grabowski [11], in particular, has shown analytically that the change in shaft compliance, and hence the dynamic response due to the asymmetry, is relatively insensitive to crack size until the crack depth is approximately 10% of the shaft diameter. It was estimated that the first observed increase in vibration level corresponded to a transverse crack approximately 3-4 inches deep (shaft diameter near midspan was approximately 40 inches).

Rotor NDE and Crack Identification

The rotor was subsequently examined by ultrasonic inspection, and two transverse cracks were identified near the midspan of the double flow LP rotor. Both cracks were under the inlet edge of the first shrunk-on turbine wheel bushing on the governor end. These cracks were later identified by destructive sectioning to be approximately 180° apart and to exhibit the dimensions shown in Figure 25. The cracks were located across the two shaft keyways used to antirotate the bushing to the shaft, and propagated circumferentially along the edge of the contact area between the bushing and the shaft. The circumferential propagation of the cracks was generally in a direction opposite to the rotation, which is consistent with fatigue cracks propagated via rotating bending. The crack surfaces revealed bench marks characteristic of changing stress or cyclic frequency conditions, and the spacing of the observed fatigue striations suggested propagation by HFF.

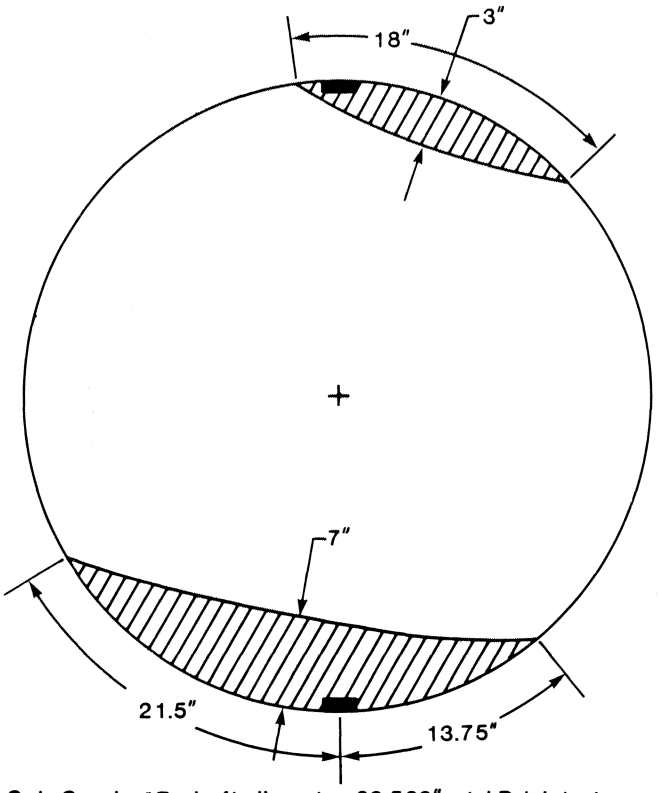

Figure 25. Representation of 320 MW Steam Turbine Shaft Transverse Cracking.

Crack Propagation Analysis

A fatigue crack propagation analysis was conducted in order to understand the crack growth mechanism. Linear elastic fracture mechanics calculations of crack growth were performed by integration of the shaft material's (Ni-Cr-Mo-V) growth rate law over the range of crack driving forces to obtain the crack progression between some initial size and final size.

The crack driving force is conveniently characterized by the crack-tip stress intensity factor (ΔK), which is proportional to the nominal stress range ($\Delta\sigma$), the square root of the crack size (a), and the specific crack and part geometry. To compute the specific magnitude of the steady (K_s) and cyclic (ΔK) crack driving forces for the crack shape modeled in Figure 25, a general-purpose fracture mechanics computer program, BIGIF [16], was utilized. BIGIF was used to accurately compute K_s and ΔK for the more complex stress distribution near the shaft surface. This distribution is affected by the stress concentration associated with the diameter change, fillet radius, and shrunk-on bushing contact stress.

The rate of fatigue crack growth in rotors made from Ni-Cr-Mo-V low alloy steels has been studied by various investigators. At low values of ΔK, the crack growth rate drops, and eventually a threshold value of $\Delta K = \Delta K_{th}$ is reached, below which fatigue crack growth does not occur. The fatigue threshold (ΔK_{th}) is also dependent on the ratio of steady stress (σ) to cyclic stress ($\Delta\sigma$), or on the ratio of K_s to ΔK [17].

The nominal cyclic stresses during steady state operation were estimated by the manufacturer to be ± 1.6 ksi (or $\Delta\sigma = 3.2$ ksi), excluding misalignment. During the deslagging operation, the steam temperature is quickly reduced by 100-150°F, and the shaft surface is cooled relative to the bore, setting up a radial temperature gradient which introduces large surface tensile stresses.

Utilizing BIGIF, the crack driving force (ΔK) was calculated, and the increase in crack depth caused by rotating bending during the periods of the high steady stresses produced during deslagging was determined. The results are shown in Figure 26.

Because the 1800 rpm turbine speed introduces fatigue cycles very quickly (1800 × 60 min/hr × 24 hr/day = 2.6 million cycles per day), crack growth could not have proceeded continuously during normal operation for a crack of the observed size. Such a crack would have grown quickly to a size where the rotor would have failed. The reason that cracking does not occur during normal operating conditions is that ΔK is below the material's *apparent* threshold, considering prior loading history [18]. Fatigue crack growth did not occur under steady-state operation in this case, because the high steady stress which caused fatigue crack growth during deslag also served as an overload, increasing the effective threshold above which fatigue crack growth could occur. The larger the relative overload, the higher the apparent threshold for subsequent crack growth. Details of this analysis are presented in Reference 19.

Correlation of Crack Growth and Vibration Increase

A correlation of increasing vibration level during deslag cycles with analytically predicted crack growth was performed. As previously shown in Figure 24, the amplitude of the second harmonic vibration was observed to be near a maximum for a period of approximately three hours. The total number of deslag operations performed on the 320 MW unit between installation and the time when such procedures were eliminated was approximately 1100. Using the 3-hour estimate for each, the total number of high thermal stress state cycles can thus be calculated as

$$1100 \text{ operations} \times 3 \text{ hours} \times \frac{1800 \text{ cycles}}{\text{min}} \times \frac{60 \text{ min}}{\text{hr}} = 356 \times 10^6 \text{ cycles}$$

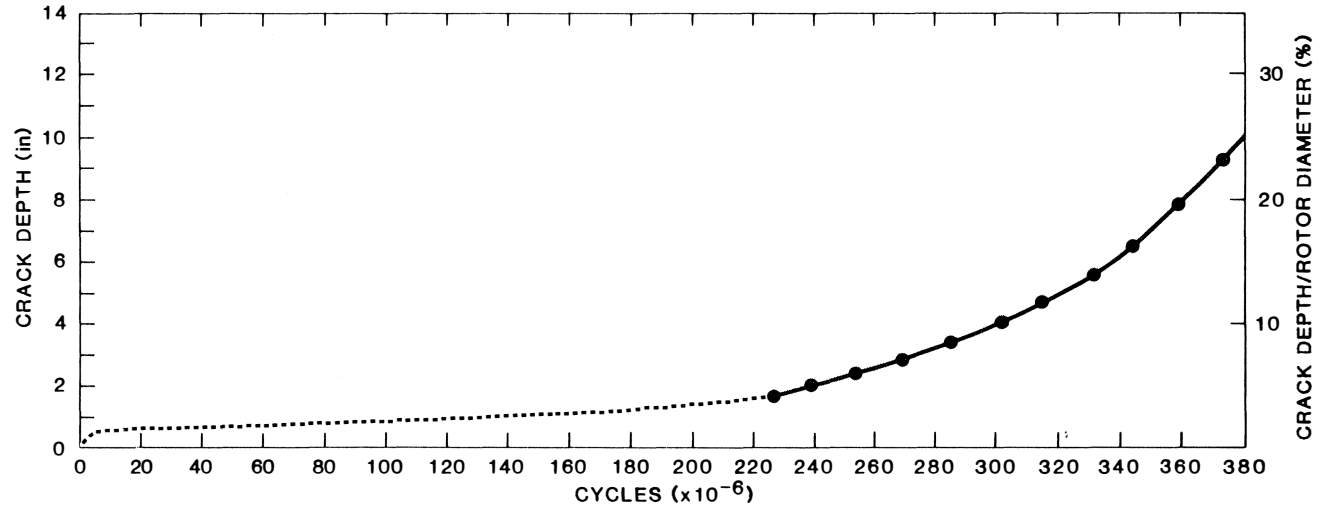

Figure 26. Transverse Crack Growth Rate Due to Deslag Thermal Transients Predicted Using BIGIF Transverse Crack Model.

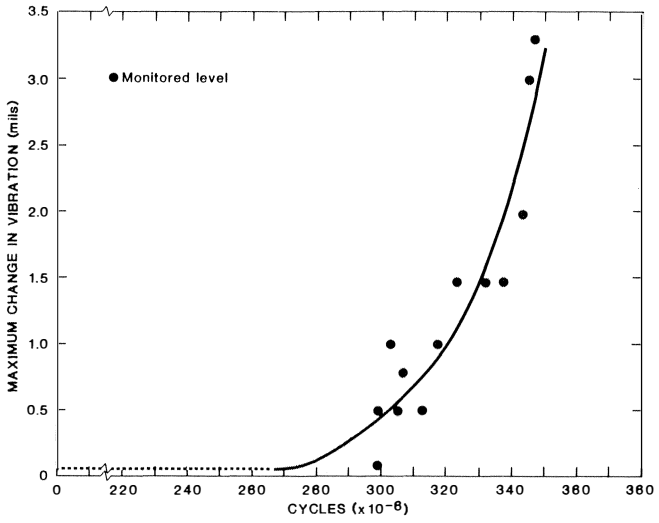

Figure 27. Maximum Changes in LP Turbine Bearing Cap Vibration During Deslag as a Function of Total Number of Cycles at Thermal Transient Stress State.

The calendar period over which these cycles occurred was reviewed and correlated to the maximum recorded increase in vibration during selected deslag operations. The form of the recorded data is unfiltered peak-to-peak displacement, in mils, as sensed on the No. 1 bearing cap in the vertical direction. A curve fit of these data as a function of cycles under the thermal transient conditions is shown in Figure 27.

Figure 28 shows that the point at which the change in vibration becomes recognizable corresponds to a crack depth between 3 and 4 inches, or between 8% and 10% of the shaft diameter. This correlates very well with the crack depth (10% of rotor diameter) predicted analytically by Grabowski [20] as necessary for significant increase in rotor vibration response.

Cracked Shaft Monitoring

In addition to the simple vibration/crack growth correlation approach presented herein, research is currently ongoing under EPRI funding to develop a complete steam turbine shaft vibration monitoring system that can be used to detect the presence of transverse cracks. This research program is directed toward quantitative diagnostics, which would allow the prediction of crack sizes. Rotor dynamic computer programs are also under development to allow diagnostic simulation of

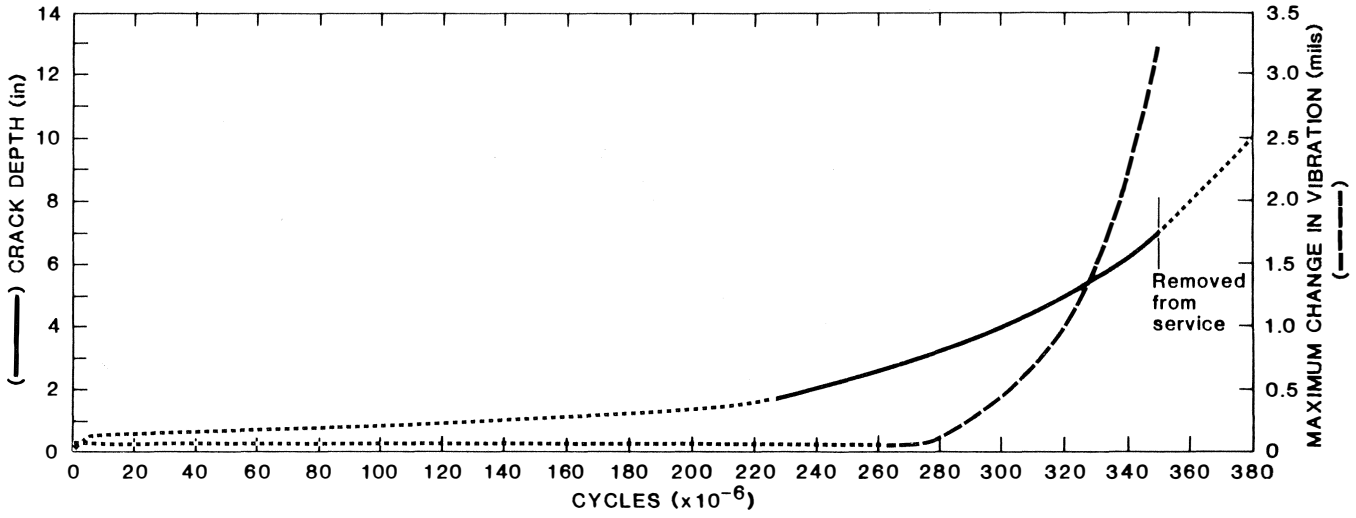

Figure 28. Correlation of Maximum Change in LP Turbine Bearing Cap Vibration During Deslag With Predicted Rotor Crack Growth.

the effect of transverse cracks on turbine rotor response. Such analysis tools could predict the onset of rotor instability due to transverse cracks, even though the cracks may not have propagated to a critical size.

CONCLUSIONS

Examples of three prevalent failure mechanisms in large steam turbine rotors have been presented.

Bore cracks, which propagate under LCF, do not produce variations in unit operational characteristics which may be quantifiably analyzed at this time for in-service crack detection. One utility reported a change in balance and vibration sensitivity with temperature, but no quantitative correlation has been developed. Research is currently ongoing to develop such in-service monitoring with the possibility of analyzing both radial and torsional rotor response, but it will be some time in development. The current technology of ultrasonic flaw detection, combined with fracture mechanics analysis, represents the major protection against rotor burst available to operators. Such analyses allow the operator to retire a rotor for cause, and not solely on the manufacturer's recommended design life.

Disk cracks, which may initiate and propagate due to stress corrosion, likewise produce no correlated changes in rotor dynamic response. Research is presently being conducted under EPRI funding to develop acoustic doppler techniques for remotely monitoring blade vibration. To the extent that disk cracking may affect blade response, especially at the blade attachments, some means of remote sensing may be developed in the future. However, the current technology of focused eddy current inspection, in combination with crack growth rate calculations, to establish safe inspection intervals and disk remaining life is available and may be important in preventing future catastrophic failures.

Shaft transverse cracks, on the other hand, can produce unit vibrational changes which may be correlated with the presence of a crack and subcritical crack growth. Here, also, EPRI is funding research to develop a monitoring system to detect and quantify the extent of crack growth. However, such monitoring will not stand alone and should be used in addition to ultrasonic inspections and crack growth/rotor lifetime analyses to prevent catastrophic failure and to allow safe utilization until replacement or retirement for cause becomes an issue.

REFERENCES

1. Bush, S. H., "Reassessment of Turbine-Generator Failure Probability," Nuclear Safety, *19*, p. 681 (1978).
2. Kramer, L. D. and Randolph, D., "Analysis of TVA Gallatin No. 2 Rotor Burst. Part I—Metallurgical Consideration," In R. M. Curran, ed., *1976 ASME-MPC Symposium on Creep-Fatigue Interaction*, G00112, also, Weisz, E. A., "Part II—Mechanical Analysis," Ibid. (1976).
3. Burska, C. D., Collins, R. V., Saez, J., Schaefer, J. E., and Takhar, J. S., "Run-Retire Decision on a 20-Year-Old L.P. Turbine Rotor Based on Boresonic and Material Test Results and Fracture Mechanics Analysis," Proceedings of the 41st American Power Conference, Chicago, Illiniois (1979).
4. Nair, P. K., Pennick, H. G., Peters, J. E., and Wells, C. H., "Reliability of Steam Turbine Rotors, Task 1: Lifetime Prediction Analysis System," EPRI Report NP-2661 (1982).
5. Landes, J. D., and Begley, J. A., "A Fracture Mechanics Approach to Creep Crack Growth," In *Mechanics of Crack Growth*, ASTM STP 590 (1976).
6. Atluri, S. N., Georgia Institute of Technology, private communication (1980).
7. Lyle, F. F. and Burghard, H. C., "Steam Turbine Disk Cracking Experience, Vol. 1: Data Summaries and Discussion," EPRI NP-2429 (1982).
8. Rau, C. A., Hopkins, S. W., Besuner, P. M., Frandsen, J. D., and Grover, J. L., "Failure Analysis of the Oak Creek Unit-3 Low Pressure Disk Burst," FaAA-78-11-3 (1978).
9. Rau, C. A., Besuner, P. M., and Sorenson, K. G., "Role of Micromechanical Models in Risk Analysis," Metals Science, p. 463 (August-September 1980).
10. Brown, S. D., et al., "Steam Turbine Rotor Reliability—Task Details," EPRI Report NP-923 (1978).
11. Grabowski, B., "The Vibrational Behavior of a Turbine Rotor Containing a Transverse Crack," Journal of Mechanical Design, Trans. ASME, *102*, pp. 140-146, (1980).
12. Mayes, I. W., "Crack Propagation in Rotating Shafts," ASME 77-DET-164 (1977).
13. Mayes, I. W., and Davies, W. G. R., "Method of Calculating the Vibrational Behaviour of Coupled Rotating Shafts Containing a Transverse Crack," Institute of Mechanical Engineering Conference Publication 1980-4, Second International Conference on Vibrations in Rotating Machinery, Cambridge, England, pp. 17-27 (1980).
14. Okah-Avae, B. E., "Analogue Computer Simulation of a Rotor System Containing a Transverse Crack," Simulation, *31*, 6, pp. 193-198 (1978).
15. Zrebarth, H. and Baumgartner, B. J., "Early Detection of Cross-Sectional Rotor Cracks by Turbine Shaft Vibration Monitoring Techniques," Joint Power Generation Conference, 81-JPGC-Pwr-20 (1981).
16. Besuner, P. M., Rau, S. A., Davis, C. S., Rogers, G. W., Grover, J. L., and Peters, D. C., "BIGIF: Fracture Mechanics Code for Structures—Introduction and Theoretical Background—Manual 1," EPRI NP-1830 (April 1981).
17. Hopkins, S. W. and Rau, C. A., Jr., "Prediction of Structural Growth Behavior Under Fatigue Loading," *Fatigue Crack Growth Measurements and Data Analysis*, ASTM STP 738 (1981).
18. Hopkins, S. W., Rau, C. A., Jr., Leverant, G. R., and Yuen, A., "Effect of Various Programmed Overloads on the Threshold for High-Frequency Fatigue Crack Growth," *Fatigue Crack Growth Under Spectrum Loads*, ASTM STP 595 (1976).
19. Rogers, G. W., Rau, C. A., Jr., Kottke, J. J., Menning, R. H., "Analysis of a Turbine Rotor Containing a Transverse Crack at Oak Creek Unit 7," *Rotor Dynamic Instability Problems in High Performance Turbomachinery*, NASA Publication 2250, p. 33 (1982).
20. Grabowski, B., "Shaft Vibrations in Turbomachinery Excited by Cracks," *Rotor Dynamic Instability Problems in High Performance Turbomachinery*, NASA Publication 2250, p. 81 (1982).